Science Advances
AAAS

advances.sciencemag.org/cgi/content/full/6/30/eaba4275/DC1

Supplementary Materials for

Realization of an intrinsic ferromagnetic topological state in $MnBi_8Te_{13}$

Chaowei Hu, Lei Ding, Kyle N. Gordon, Barun Ghosh, Hung-Ju Tien, Haoxiang Li, A. Garrison Linn, Shang-Wei Lien, Cheng-Yi Huang, Scott Mackey, Jinyu Liu, P. V. Sreenivasa Reddy, Bahadur Singh, Amit Agarwal, Arun Bansil, Miao Song, Dongsheng Li, Su-Yang Xu, Hsin Lin, Huibo Cao, Tay-Rong Chang*, Dan Dessau*, Ni Ni*

*Corresponding author. Email: nini@physics.ucla.edu (N.N.); dessau@colorado.edu (D.D.); u32trc00@phys.ncku.edu.tw (T.-R.C.)

Published 22 July 2020, *Sci. Adv.* **6**, eaba4275 (2020)
DOI: 10.1126/sciadv.aba4275

This PDF file includes:

Note I: Single crystal growth and structure determination

The systematic way we did to find out the growth window for each phase is: since the growth window for $MnBi_8Te_{13}$ is quite narrow, we used the same furnace for all trials to avoid furnace to furnace temperature variation. In each trial, we first set the decanting temperature to be T1, we then decanted the growth by a pre-warmed centrifuge, if we got no liquid flux out during the centrifuging process, it meant T1 was so low that all materials were in the solid state at T1. Then in the next growth, we increased the decanting temperature a little to T2 (this could be done by carefully moving the synthesis in different location inside the furnace), then if we got $MnBi_6Te_{10}$ after decanting, this meant T2 is too high and we missed the growth window of $MnBi_8Te_{13}$. Then we decreased the decanting temperature to be between T1 and T2, by this, after decanting, we could get $MnBi_8Te_{13}$. During this trial process, if we got $MnBi_4Te_7$, that just meant the decanting temperature was way too high. Usually, in the successful $MnBi_8Te_{13}$ growth, we saw a few single crystals on top of a chunk inside the crucible. This is because the decanting temperature is so close to the solidification temperature that during the process of decanting, only the liquid on the top was successfully separated from the $MnBi_8Te_{13}$ crystals.

Powder X-ray diffraction pattern and the Rietveld refinement of $MnBi_6Te_{10}$ are shown in Fig. S1. Nice agreement is achieved.

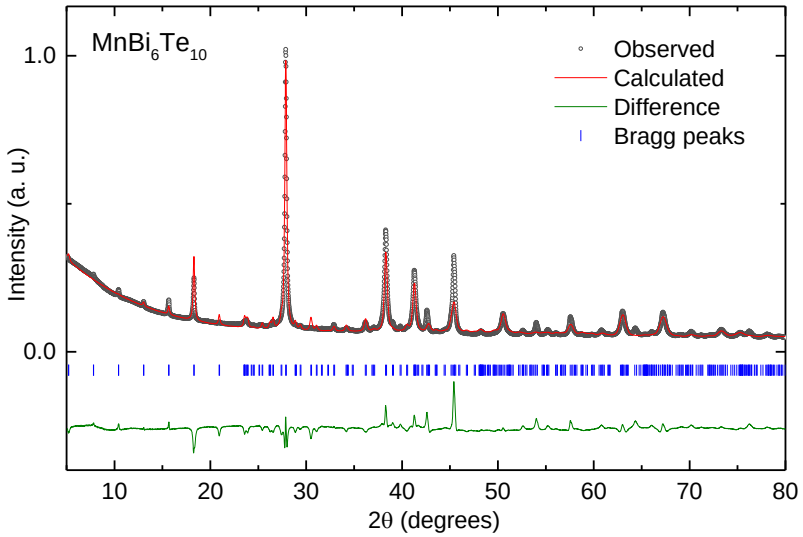

Figure S1. Powder X-ray diffraction and the refinement of $MnBi_6Te_{10}$.

Table S1 and S2 summarize the crystal structures of $MnBi_6Te_{10}$ and $MnBi_6Te_{10}$ based on our refinement on the powder X-ray patterns.

Table S1. Rietveld refinement results of powder $MnBi_6Te_{10}$ and $MnBi_8Te_{13}$ at room temperature.

Results	$MnBi_6Te_{10}$	$MnBi_8Te_{13}$
Space group	R-3m	R-3m
a (Å)	4.3711(3)	4.37485(3)
c (Å)	101.825(8)	132.416(2)
V ($Å^3$)	1684.8(2)	2194.81(4)
Reliability factor Rp	7.00	2.25

Table S2. Atomic coordinates and equivalent isotropic displacement parameters of $MnBi_6Te_{10}$ and $MnBi_8Te_{13}$ at room temperature. For $MnBi_6Te_{10,}$ all isotropic thermal parameters are fixed to be 0.8.

$MnBi_6Te_{10}$					
Atom	Site	x	y	z	B_{iso} ($Å^2$)
Mn1	3a	0	0	0	0.8
Bi1	6c	0	0	0.2357(1)	0.8
Bi2	6c	0	0	0.2953(1)	0.8
Bi3	6c	0	0	0.4704(1)	0.8
Te1	6c	0	0	0.0535(2)	0.8
Te2	6c	0	0	0.1154(2)	0.8
Te3	6c	0	0	0.1790(2)	0.8
Te4	6c	0	0	0.3490(2)	0.8
Te5	6c	0	0	0.4133(2)	0.8

$MnBi_8Te_{13}$					
Atom	Site	x	y	z	B_{iso} ($Å^2$)
Mn1	3a	0	0	0	0.8
Bi1	6c	0	0	0.18221(4)	0.31(7)
Bi2	6c	0	0	0.22824(5)	0.31(7)

Bi3	6c	0	0	0.36168(5)	0.31(7)
Bi4	6c	0	0	0.40865(6)	0.31(7)
Te1	6c	0	0	0.04172(8)	1.6(1)
Te2	6c	0	0	0.0897(1)	1.6(1)
Te3	6c	0	0	0.13757(8)	1.6(1)
Te4	6c	0	0	0.2707(1)	1.6(1)
Te5	6c	0	0	0.32131(7)	1.6(1)
Te6	6c	0	0	0.4524(1)	1.6(1)
Te7	3b	0	0	0.5	1.6(1)

Note II: ARPES data: temperature dependence

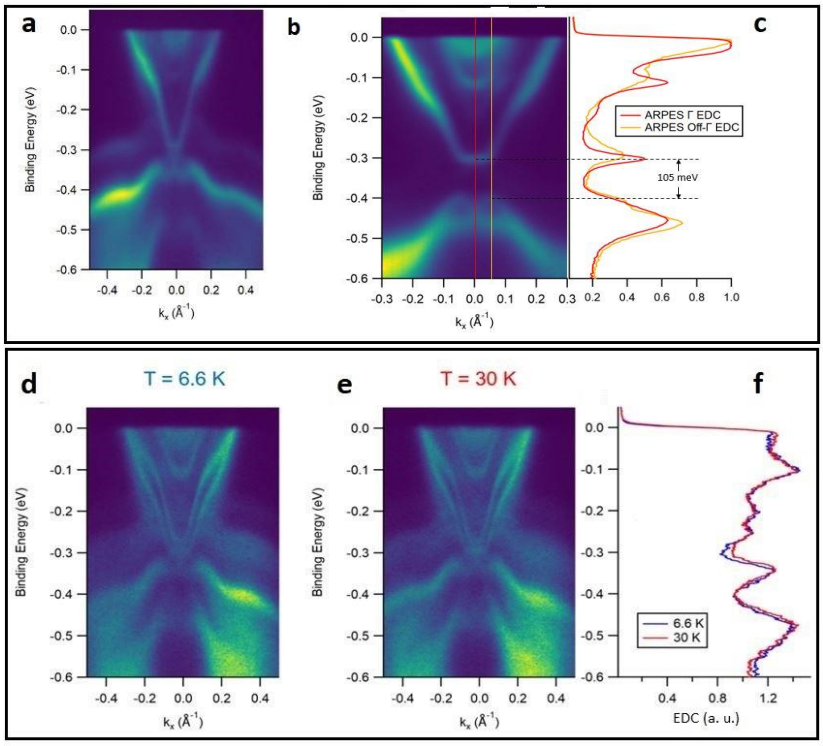

Figure S2. The experimental ARPES data: **a-b** The experimental ARPES *E-k* spectrum cut along the $M \rightarrow \Gamma \rightarrow M$ high symmetry direction for QL_2 (**a**) and QL_1 (**b**) terminations at 12 K. **c** Energy distribution curve (EDC) of the spectra **b**. The inferred surface gap is about 105 meV. **d-e** The experimental ARPES *E-k* spectrum cut along the $M \rightarrow \Gamma \rightarrow M$ high symmetry direction at 6.6 K (**d**) and 30 K (**e**). **f** Energy distribution curve (EDC) at the Γ point of spectra **d** and **e**.

To check the evolution of the surface state above and below the transition temperatures, ARPES data were measured at 6.6 K and 30 K. Due to the slightly bigger beam spot at this instrument, the spectra are a combination of the spectra arising from different terminations; however, we can identify the terminations present in the spectra to be $QL_1 + QL_2$ when we compare the combined spectra with the ones we measured for each termination at 12 K with the smaller beam spot. Furthermore, we found that the spectra taken at 6.6 K and 30 K are very similar in terms of the size of the gap, except for thermal broadening of the electrons. This has been observed in various magnetic topological insulators, including $MnBi_2Te_4$, $MnBi_4Te_7$, $MnBi_6Te_{10}$, etc. The origin of it is under hot debate.

Note III: The bulk band structure without atomic relaxation

Table S3 The number of occupied bands of the even and odd parity eigenvalues at the eight TRIM points.

Γ_i	(0,0,0)	(π,0,0)	(0,π,0)	(0,0,π)	(π,π,0)	(0,π,π)	(π,0,π)	(π,π,π)
n^+_{occ}	65	67	67	67	63	63	63	67
n^-_{occ}	60	58	58	58	62	62	62	58

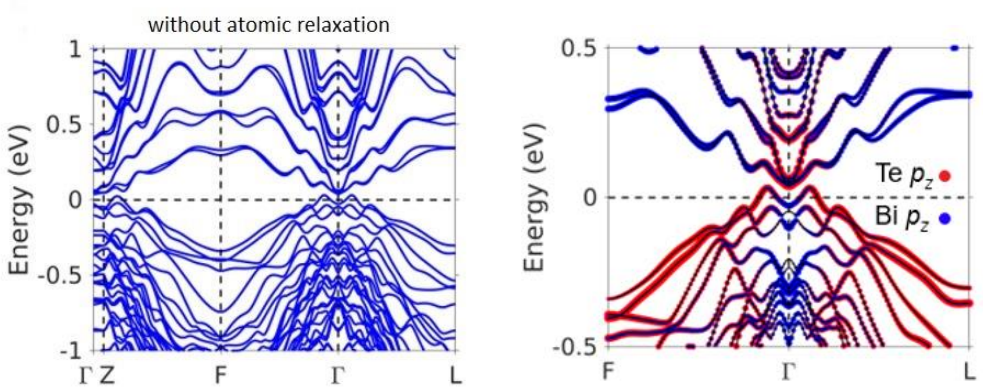

Figure S3. Bulk band structure of $MnBi_8Te_{13}$ calculated using the experimental lattice parameters and atomic positions. Bulk band structure of $MnBi_8Te_{13}$ in the out-of-plane FM configuration with spin-orbit coupling (SOC) and correlation parameter *U* included.

Figure S3 shows the band structure calculation where experimental lattice parameter and atomic positions without atomic relaxation are used. We found a continuous energy gap

separating the highest valence band (VB) and the lowest conduction band (CB) throughout the BZ. This contradicts with the observation from ARPES. It is noted that, in calculations with or without atomic relaxation, the characteristics of band inversion and the topology of whole system remain the same, i.e., an FM axion state.

Note IV: The understanding of the hybridization gap from DFT calculations

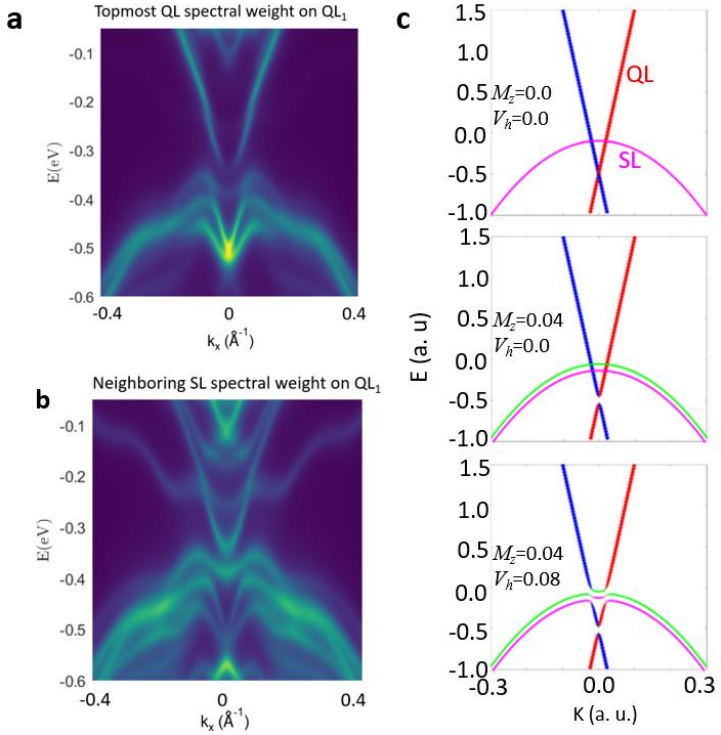

Figure S4. Theoretical calculations on the hybridization gap. a-b The calculated spectral weight within the topmost QL (**a**) and the nearest-neighboring SL (**b**) on QL_1 termination. **c** A surface *k.p* model to display the evolution of the band hybridization between QL and SL.

To further understand the hybridization gap in QL_1 termination, we plot the spectral weight within the topmost QL and the nearest-neighboring SL, as shown in Fig. S4 **a,b**. We see the conduction band is mainly from the surface state of the topmost QL while the valence band is from the nearest-neighboring SL. This feature demonstrates that this gap is induced from the hybridization effect between these two layers (*50,51*). This hybridization gap occurs at the surface of the system, which can be regarded as an effectively 2D band inversion.

To better show the band inversion feature in QL_1 termination, we construct a surface $k \cdot p$ model to display the evolution of the band hybridization between QL and SL, as shown in Fig. S4 c.

The effective Hamiltonian reads,

$$H_s = \begin{pmatrix} m_z & ivk_x - vk_y & V_h & 0 \\ -ivk_x - vk_y & -m_z & 0 & V_h \\ V_h & 0 & -\frac{\hbar k^2}{2m^*} + m_z + c & 0 \\ 0 & V_h & 0 & -\frac{\hbar k^2}{2m^*} - m_z + c \end{pmatrix}.$$

The basis states are ordered as $\{|QL\uparrow\rangle, |QL\downarrow\rangle, |SL\uparrow\rangle, |SL\downarrow\rangle\}$. Here m^* is the electron effective mass of electron in the SL, c is the Fermi energy measured from the SL band, v is the Fermi velocity of the band of QL, and ↑ (↓) denotes the spin up(down) states. The m_z is the Zeeman splitting energy, and the V_h term is a parameter describing the hybridization strength between QL and SL. Figure S4**c** presents the evolution of the band structure. At the beginning, as $m_z = 0$ and $V_h = 0$, we see a spin polarized Dirac band from QL (the red and blue dots indicate spin up and down, respectively) and the quadratic band from SL. Upon including the magnetic interaction M_z in the middle panel, the Dirac band opens a mass gap and the quadratic band displays the Zeeman splitting character (the green and purple dots indicate spin up and down character, respectively). In the final step in the bottom panel in which the interaction between QL and SL is switched on, the band dispersion shows a clear hybridization gap with band inversion features, which is consistent with DFT surface band dispersion in $MnBi_8Te_{13}$ with QL_1 termination.